Hindawi
Advances in Materials Science and Engineering
Volume 2022, Article ID 7003227, 16 pages
https://doi.org/10.1155/2022/7003227

Research Article

Creep Behaviors of Interlayers around an Underground Strategic Petroleum Reserve (SPR) Cavern in Bedded Salt Rocks

He Chen,[1,2] Huihua Peng,[1,2,3] Jian Duan,[1,3] Jun Wang,[1,3] Shengnan Li,[1,3] and Yuejing Yang[1]

[1]*Department of Building Engineering, Hunan Institute of Engineering, Xiangtan, Hunan 411104, China*
[2]*State Key Laboratory of Coal Mine Disaster Dynamics and Control, Chongqing University, Chongqing 400044, China*
[3]*Hunan Provincial Key Laboratory of Intelligent Disaster Prevention-Mitigation and Ecological Restoration in Civil Engineering, Hunan Institute of Engineering, Xiangtan, Hunan 411104, China*

Correspondence should be addressed to Huihua Peng; penghui-hua@foxmail.com

Received 19 September 2022; Revised 7 November 2022; Accepted 8 November 2022; Published 15 November 2022

Academic Editor: Chenggao Li

It is well known that the Strategic Petroleum Reserve in salt caverns is an important means to solve the potential petroleum shortage. However, salt mines in China are mainly lacustrine-layered structures with many mudstone interlayers. Meanwhile, the acid value of extracted crude oil has been increasing in recent years. The acid erosion of salt cavern interlayers by crude oil would affect the safety of bedded salt cavern oil storage. Therefore, combined with acoustic emission technology, the multistage creep mechanical behaviors of natural mudstone interlayer samples and the mudstone interlayer samples treated by oil erosion are studied in this paper. The internal structures of interlayer samples before and after oil erosion were systematically analyzed by SEM. The results show that petroleum acid (naphthenic acid) plays a significant deterioration role in the mechanical properties of mudstone interlayers during the petroleum reserve process. Compared with the uncorroded samples, the mudstone interlayers after oil erosion show obvious brittle failure characteristics. At low stress levels, the axial strain grows stepwise and the lateral strain is smaller than the axial strain. At high stress levels, however, the lateral creep is obviously higher than the axial creep. A large number of AE signals were generated at the initial loading stage for different stress levels. After the creep stabilized, the AE signals were significantly reduced. During the process of petroleum erosion, the internal pores in rocks continued to develop with the dissolution of many mineral particles. This suggests that crude oil storage in the bedded salt rocks could accelerate the deterioration of the surrounding rocks via erosion. This paper could provide basic research data and a reference for the construction of oil storage in the bedded salt rocks.

1. Introduction

As a strategic resource, petroleum is dominant in the world's energy structure. Due to the outbreak of the new crown epidemic in 2020, the global economic blockade has severely disrupted international oil trade activities and caused an imbalance in the structure of oil supply and demand. As the energy lifeline of the country [1], the oil crisis will adversely affect the economic security and social stability [2]. Because salt rock has excellent characteristics, such as low permeability, good creep performance, and stable chemical properties, it is recognized internationally as a good place for energy storage [3–5]. The United States has stored 62 Strategic Petroleum Reserve (SPR) caverns in four different places in Texas and Louisiana, accounting for 90% of its oil reserves. About 42% of Germany's oil is stored in underground salt caverns [6]. According to the third stage plan of China's strategic oil reserves, the government will vigorously support the construction of strategic oil reserve in underground salt caverns, such as in Jiangsu Province [7].

Most of the salt caverns' energy storage facilities are built in huge salt domes. However, the salt mines in China are mostly lacustrine sedimentary structures, which are characterized by many interbedded interlayers and a thin single

interlayer [8–10]. Due to the great differences between the geological conditions of salt rocks in China and those in foreign countries, it is impossible to replicate and apply existing research achievements in foreign countries. Therefore, it is necessary to study the basic theories and technologies of layered rock salt oil depot construction based on the specific geological conditions in China. A sketch map of the salt rock in oil storage caverns in China, Europe, and the USA is shown in Figure 1. The existence of many mudstone interlayers makes the physical and mechanical properties of the salt mine more complex, such as uncoordinated strain caused by strength differences between layers. During the long-term creep of the salt cavern, lateral tensile failure of the interlayer occurs before that of the salt rock, although its strength is greater than that of the salt rock [11]. The bedding plane is a lithologic transition zone between the salt rock and the interlayer. Because of the stress concentration, the bedded salt rock produces nonconforming deformation. The creep characteristics of the layered salt rock are mainly derived from the salt rock part, in which the interlayer has a good inhibitory effect on the creep deformation of the salt rock [12]. The mechanical properties of the interface between salts and interlayers are between the salt rocks and the interlayers [13]. Ślizowski and Lank [14] studied the rheological properties of the mudstone interlayer in the bedded salt rock and believed that the mudstone interlayer with higher rock salt content (salt content of 70%~80%) is a good medium for nuclear waste storage. Li and Yang [15] proposed a three-dimensional extended Cosserat medium constitutive model of layered rock salt and used it for the stability analysis of underground salt caverns. Zhou et al. [16] established a fractional-order model of salt rock, which can provide a certain reference basis for the judgment of salt cavity failure. Yang et al. [17] proposed a three-dimensional geomechanical model to evaluate the feasibility of using underground gas storage (UGS) in layered rock salt caverns and verified its accuracy through on-site sonar measurement of on-site data. In the process of leaching cavities by water dissolution, brine intrusion has a significant weakening effect on the compressive strength of the mudstone interlayer. Collapse is caused by the swelling of mudstone, which has a certain impact on the safety of construction [18, 19]. When the surrounding rock exceeds its strength limit, it is very likely to induce a series of disasters such as crack expansion and oil leakage, which will lead to environmental problems such as groundwater pollution.

In recent years, domestic crude oil has entered the secondary and tertiary exploitation period, and the acid value of crude oil in China has also increased year by year, and the import of high-acid crude oil is also increasing [20]. The Bohai Sea is the region with the greatest potential for increasing the production of high-acid crude oil in China. The TAN of PL 19-3 crude oil reaches 6.02 mg KOH/g, which is a typical low sulfur, high acid crude oil. Although oil can stably contact rock salt for a long time, the mechanical properties of the mudstone interlayer in contact with oil are still unclear. In particular, changes in operating pressure during the processes of injection and production will accelerate the destruction of the surrounding rock. Coupled with the chemical erosion of oil on the mudstone interlayer, the safety status is even more difficult to predict. In view of the fact that there is no precedent for salt cavern oil storage in China, there is a lack of theoretical basis and practical experience in layered salt rock, such as the mechanical properties of interlayers. Therefore, understanding the creep mechanical behavior of mudstone interlayers is a prerequisite for the design of operating conditions during the operation of the salt cavern oil storage.

In this paper, the mudstone interlayer in the salt mine area of Jiangsu is selected as the research object, and multilevel creep tests are carried out on the natural mudstone interlayer sample and the mudstone interlayer sample eroded by acid oil. Under different stress levels, acoustic emission signals are collected synchronously from the initial loading stage to the steady creep stage. Through the scanning electron microscope (SEM) test, the internal microstructure changes before and after the oil erosion were analyzed. Based on the test results, the creep characteristics of a natural sample and a sample after oil erosion were studied. By comparing the two samples, the influence of oil erosion on the damage evolution and creep characteristics of the mudstone interlayer during the operation process of the salt cavern oil storage is analyzed. This study provides a theoretical and experimental basis for the construction and stability analysis of an underground oil storage cavern in bedded rock salt.

2. Experimental Scheme

2.1. Sample Preparation. The mudstone cores were taken from the target stratum of the salt mine in Jiangsu Province at a depth of about 500–2000 m. The target stratum is rich in salt resources with high-grade deposits, and stable salt caverns are formed after mining, which has the geological conditions for large-scale construction of underground salt cavern. The cores show different colour textures due to the varying compositions and contents (mainly limestone ($CaCO_3$) and hard gypsum ($CaSO_4$)) and the surface of the specimens being predominantly dark grey and grey, typical of muddy inclusions. The object of this work is to investigate the creep behavior of the mudstone interlayers before and after oil erosion. Herein, the samples were wire-cut by SM 150 sample manufacturer equipment. This preparation method could produce samples with high accuracy and less damage to the rock samples. The samples were machined into cylindrical samples with a diameter of approximately 50 mm and a height of 100 mm, and the accuracy is controlled within 0.2 mm. All samples meet the requirements of the International Society for Rock Mechanics (ISRM) (ISRM, 2007). The experiment was divided into two groups, i.e., the natural mudstone samples without oil erosion and the oil-eroded mudstone samples. To ensure the comparability of test results, the number of samples in each group was 3.

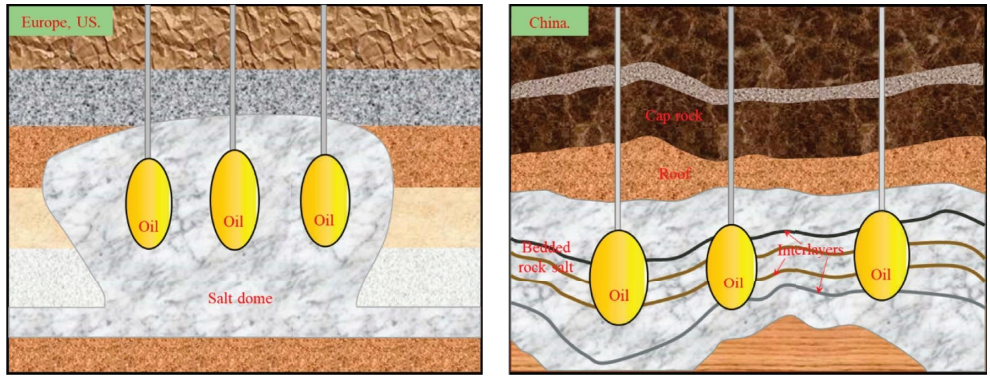

(a) (b)

Figure 1: Salt caverns in different salt formations. (a) SPR caverns in salt dome. (b) SPR caverns in bedded salt rock.

2.2. Sample Pretreatment

2.2.1. TAN Preparation of Oil. Crude oil is a complex mixture of many components, and its chemical composition is very complex, consisting mainly of alkanes, cycloalkanes, and aromatic hydrocarbons. During the operation of salt cavern oil storage, petroleum acids in crude oil could react chemically with mineral particles in the muddy interlayers in the surrounding rock, causing some erosion damage to the cavity's surrounding rock [19]. The acidity of crude oil is usually expressed by its total acid number (TAN), which is the milligrams of KOH consumed to neutralize acidic substances in a 1 gram of crude oil sample. This parameter represents the total content of acidic substances in crude oil.

With domestic crude oil having entered the second and third exploitation periods, the acid value in the crude oil is also increasing year by year. With reference to the Penglai 19-3 crude oil discovered in recent years, its acid value is 6.02 mg KOH/g. In this test, sour oil prepared to this standard was used instead of highly sour crude oil. TAN determination is carried out in strict accordance with the petroleum products' determination (GB/T 264–1983). Because of the complex chemical composition of crude oil, petroleum acid was selected in this experiment to avoid the interference of other impurities in crude oil. Therefore, acidic oil formulated in this ratio was used in this study instead of a high sour crude oil for the oil erosion tests. In the test, oil with an acid value of 6 mg KOH/g was used for all oil erosion tests.

2.2.2. Pore Pressure Interaction of Oil-Mudstone. To study the creep mechanical properties of the mudstone interlayer under uniaxial compression with pore pressure generated by oil, our research group independently designed an oil pore pressure erosion test device for the tests (Figure 2). The maximum pore pressure of the equipment reaches up to 30 MPa. It can simulate the pore pressure generated by oil on the rock surrounding the cavern within the SPR caverns based on the actual operating conditions of the salt cavern. The oil erosion test was carried out for mudstone interlayers at a pore pressure of 5 MPa. The immersion time was set at 7 days. The pore pressure was set according to the hydraulic

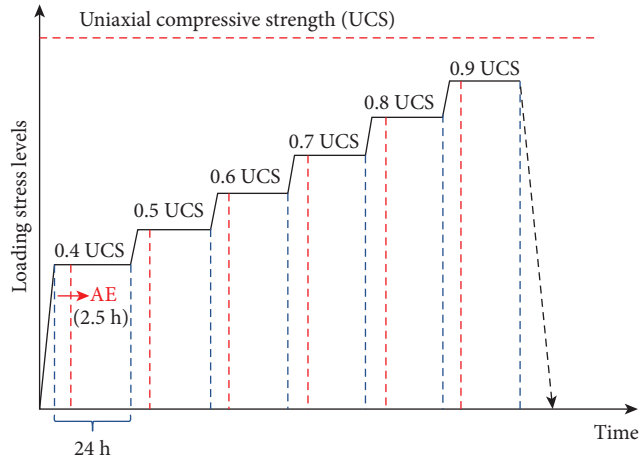

Figure 2: The loading paths of the creep tests [21].

pore pressure of the oil acting on the mudstone at a depth of 600 m. The hydraulic pressure of the crude oil on the mudstone is about 4.92 MPa ($\gamma_{oil} = 8.20$ kPa/m).

2.3. SEM Tests.

In order to analyze the changes in internal structures before and after oil erosion. First of all, a small representative rock sample was removed from the target sample after pretreatment. After the spray was completed, the sample was placed in a dry environment and sealed for storage. After the sample preparation was completed, the scanning electron microscope (SEM) Zeiss Auriga was used to observe the structural characteristics of all rock slices and then analyze the changes to the internal structures of the rock samples.

2.4. Uniaxial Compression and Creep Tests.

Uniaxial compression and creep tests were carried out using the rock mechanics test system. Acoustic emission (AE) signals were monitored synchronously during the tests, using the PCI-2 Acoustic Emission Monitor of the American Physical Acoustics Company. The tests were divided into two groups. The first group was composed of natural mudstone interlayers, and the second group was composed of mudstone

interlayers after oil-mudstone 5 MPa pore pressure interaction. The uniaxial compression experiment was carried out at a speed of 0.1 mm/min until rock failure. The obtained uniaxial compressive strength (UCS) could be used as a reference for selecting the loading stress level in creep tests. As a result, the UCS of the natural mudstone interlayer sample was 25.6 MPa, while the UCS of the sample after 5 MPa pore pressure erosion was 16.3 MPa.

Taking into account the long-term stability of the underground salt cavern oil storage, it is of great significance to identify the deformation and failure of the surrounding rocks after oil erosion. Given that there are no engineering examples of salt cavern petroleum storage reservoirs in China, at the initial stage of the study, the short-term creep characteristics of the mudstone interlayer before and after oil erosion were initially explored. In the subsequent study, the long-term creep characteristics of the mudstone interlayer will also be the main direction of research, and the influence of oil erosion on the long-term creep characteristics of the mudstone interlayer will be fully considered. Therefore, a series of uniaxial compressive creep tests were carried out, and multiple stress levels were applied to each sample until failure. The loading levels were predefined as 0.4, 0.5, 0.6, 0.7, 0.8, and 0.9 UCS. Each level lasted 24 hours. Within 2.5 hours after the start of each stage, acoustic emission signals were collected simultaneously. The loading paths of the creep test are shown in Figure 2. Here, we followed the methods of Chen et al. [21].

The ratio of the predetermined loading stress to the uniaxial compressive strength (UCS) is defined as loading ratio indicator (k), which is expressed as [22]

$$k = \frac{\sigma_a}{\sigma_{\text{ucs}}}, \tag{1}$$

where σ_a is the predefined loading stress and σ_{ucs} is the uniaxial compressive strength. Table 1 lists the loading ratios and corresponding loading stresses of the two groups of samples. This entire of the experimental procedure is presented in Figure 3.

3. Results and Discussion

3.1. Mechanical Parameters. According to the difference in strain rates, the creep process can be divided into three stages: the primary creep stage (strain rate keeps decreasing with time), the secondary creep stage (strain rate remains constant, also known as the steady-state creep stage), and the tertiary creep stage (strain rate increases rapidly until failure), as shown in Figure 4. ε_0, ε_c, and ε_t are the instantaneous strain (i.e., initial strain) and creep strain, and the total strain at each stress level, respectively, i.e., $\varepsilon_t = \varepsilon_0 + \varepsilon_c$.

3.1.1. The Evolution of Creep Strains. Figure 5 shows the uniaxial compression creep test curves of the natural sample and the sample after oil erosion (under the condition of a pore pressure of 5 MPa). At the loading moment of each stress level, the sample experienced an instantaneous elastic response, and then the creep deformation increased with time. As shown in Figure 5(a), the natural sample was loaded with 4 stress levels until creep failure occurred, and the failure occurred after 81.824 h. When the loading ratio is 0.4 to 0.6, the sample shows an obvious initial creep stage and steady-state creep stage. The axial strain increased with time, and the axial creep strain rate decreased with the increase in time. After reaching a certain time, the creep rate gradually stabilized and entered a relatively stable creep stage. As the stress level increased, the creep rate and creep deformation of the sample were different. The greater the axial stress, the faster the creep rate and the larger the corresponding creep deformation. At the last level of stress (a load ratio of 0.7), there are obviously three stages of creep deformation. After the stable creep stage, the strain rate of the sample increases rapidly, which eventually leads to the failure of the sample.

The uniaxial compression axial creep curve of the sample after oil erosion is shown in Figure 5(b). After 5 stress levels are loaded, creep failure occurs, the failure time is 98.658 h, and the failure time increases. Different from the natural sample, at each stress level, the initial creep stage of the sample after oil erosion is not obvious, and the corresponding axial deformation is small. When the loading ratio is 0.4~0.5, the axial strain increases step by step, accompanied by a large mutation, showing obvious brittle characteristics. With the increase of the stress level, the axial strain of the sample also has a large mutation change during the stress rise. When the loading ratio is 0.6 to 0.7, the axial strain curve is relatively flat, and the initial creep stage and stable creep stage of the sample are no longer obvious. At the last level of stress (the loading ratio is 0.8), the failure duration of the sample is shorter, and the transition from the stable creep stage to the accelerated creep stage is not obvious, showing the characteristics of brittle failure. In general, in the creep deformation stage, the axial creep of the sample after oil erosion is smaller than that of the natural sample, and the brittleness of the sample is enhanced. Therefore, based on engineering considerations, during the operation of the salt oil storage cavern, frequent oil injection and production should be minimized, and a constant operating pressure should be maintained, as every injection of oil makes the surrounding rock of the cavern suffer new damage.

As it can be seen from Figure 5, the lateral strain and the axial strain of the two groups of samples show the same changing trend, so they are not repeated here. It is worth noting that under different stress levels, the lateral strain of the natural sample is higher than that of axial strain. Under the last level of stress, the lateral strain and lateral strain rate are significantly higher than the axial strain. The creep characteristics of the sample after oil erosion are not obvious, and the strain is reduced. The reason for this phenomenon may be attributed to physical and chemical erosion. When the interlayer samples were eroded with the oil due to the action of pore pressure and chemical erosion, the mineral particles were eroded, thereby reducing the bonding force between the mineral particles. Therefore, during the operation of the salt cavern oil storage, when the operating pressure is low, the monitoring of the axial strain of the surrounding interlayer should be strengthened, and

Table 1: Loading ratios (k) and the corresponding loading stresses.

Loading ratios	Sample	0.4	0.5	0.6	0.7	0.8	0.9
σ_a (MPa)	Natural sample	10.24	12.79	15.34	17.89	20.44	22.99
	Sample after oil erosion	6.52	8.15	9.78	11.41	13.04	14.67

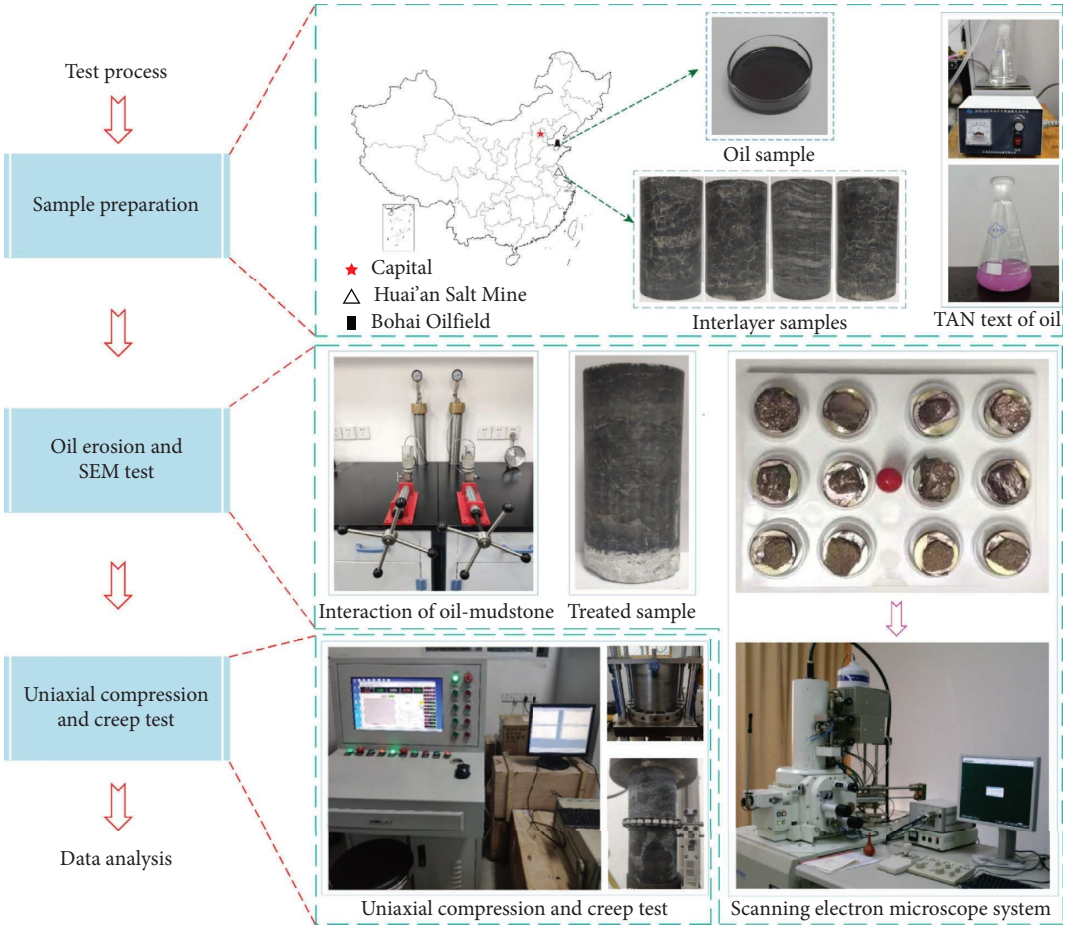

Figure 3: Experimental procedures.

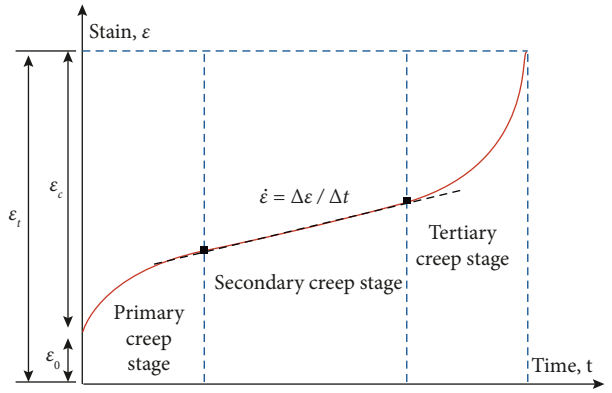

Figure 4: Typical creep curve of rock material [21].

when the operating pressure is high, the monitoring of the lateral strain of the surrounding interlayer should be strengthened.

In addition to considering the discreteness of the sample itself and the influence of the deviation in the test process, we analyzed that the internal pores of the sample continued to

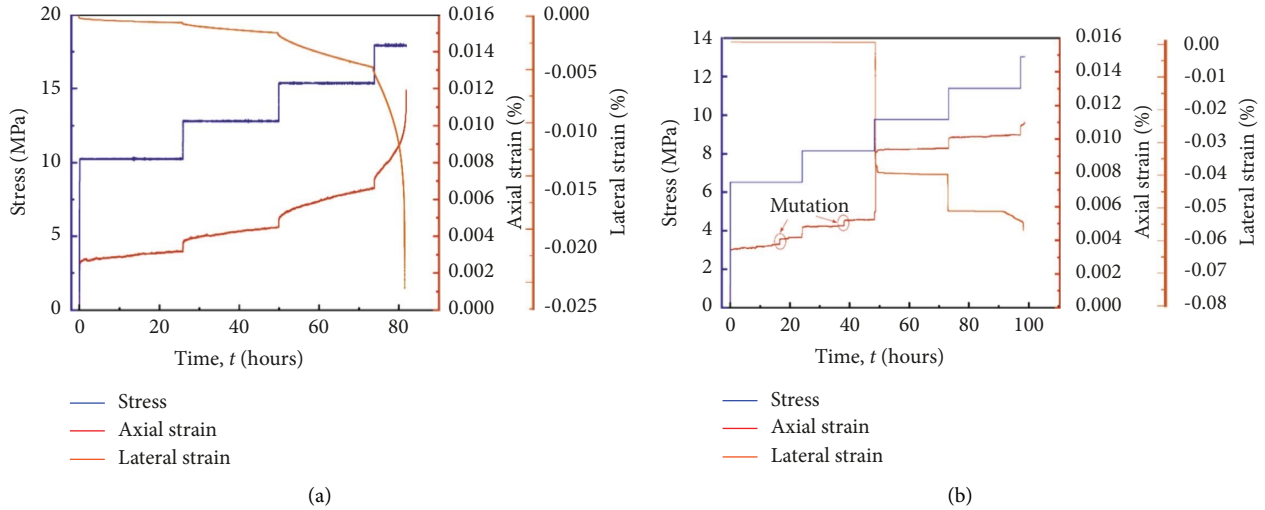

Figure 5: Creep strain curves by the step loading: (a) the natural sample and (b) the oil-eroded sample.

develop during the oil erosion process, causing significant changes in the microscopic pore structure. At the same time, the pore pressure makes it easier for oil to enter the inside of the sample, thereby accelerating the internal erosion of the sample, and many mineral particles are eroded, causing the cement between mineral particles to become friable. In the initial stage of the creep test loading, the stress level is low, the internal pores of the sample are gradually compacted, and the loose particles are continuously compacted, so that the strain grows stepwise with time, accompanied by mutation, showing the characteristics of brittle failure. Since the natural sample interlayer and the salt rock particles are connected in series, the time-varying characteristics are more obvious when subjected to axial force. When subjected to axial force, the radial strain of the sample after oil erosion is not obvious. With the increase of the stress level, the friable particles inside the sample are continuously crushed, the internal pores and defects are gradually compacted, and the axial strain develops in a stepped manner to be stable. Therefore, the time-varying characteristics of the surrounding rock under oil erosion should be fully considered when designing the operating conditions of salt cavern oil storage.

3.1.2. Steady-State Creep Strain Rate. Tables 2 to 3 list the uniaxial compressive strain parameters of the natural sample and the sample after oil erosion under different stress levels, where ε_0, ε_c and ε_t are the instantaneous strain, creep strain, and total strain at each stress level, respectively. Both the axial creep and lateral creep deformation of the sample increase with the increase of the stress level.

According to the previous study on the creep test of salt rock under multistage creep test [23], the steady state creep rate of the rock has nothing to do with the historical path of loading. Therefore, applying multistage creep loading to the same sample can not only avoid the influence of the discreteness of the sample on the test results but also analyze the changes in the steady creep rate of the rock under different stress levels.

As shown in Tables 2 to 3, with the increase in the loading stress level, the steady state creep rate of the natural sample shows an upward trend. For the sample after oil erosion, when the loading ratio is 0.4 to 0.6, the axial steady state creep rate shows two stages, that is, two stages before and after the mutation. Before the mutation, the axial steady state creep strain rate first decreased and then increased with the increase in the stress level. After the mutation, the axial steady state creep rate first increased and then decreased with the increase in the stress level. At the same time, the lateral steady state creep rate first decreases and then increases as the stress level increases. According to the consistency of axial strain and lateral strain, the author thinks that when the loading ratio is 0.4~0.5, the mutation and the creep strain at the end of the mutation will occur in the corroded parts on the end face, and the surface particles will be crushed gradually. When the loading ratio is 0.6, the mutation of the sample and the part after the mutation occurred inside the sample. From an engineering point of view, the surrounding rock interlayer near the cavern is a dangerous point. It is very important to strengthen the monitoring of creep strain and steady state creep rate here.

Figure 6 shows the strain and strain rate of a natural sample and the sample after oil erosion at the final stress level. It shows the complete creep behavior of the sample at the final stress level. Obviously, there are three creep stages in the creep process of the natural sample and the sample after oil erosion under the creep failure stress level. That is, the initial creep stage when the strain rate decreases, the steady state creep stage at a constant strain rate, and finally the accelerated creep stage. It can be clearly seen from Figure 7 that the creep duration and the creep rate in the steady state creep stage and the accelerated creep stage of the natural sample are greater than those of the sample after oil erosion. In the initial creep stage, the creep rate of the sample after oil erosion is greater than that of the natural sample. This is mainly because the internal tandem structure of the natural sample and the sample after oil erosion are different, which leads to the difference in creep duration. After the

Table 2: Creep parameters of natural sample under different stress levels.

Strain	ε	$0.4\sigma_{ucs}$	$0.5\sigma_{ucs}$	$0.6\sigma_{ucs}$	$0.7\sigma_{ucs}$
Axial strain	ε_0	2.490×10^{-3}	3.625×10^{-3}	4.930×10^{-3}	7.042×10^{-3}
	ε_c	6.773×10^{-4}	8.466×10^{-4}	1.673×10^{-3}	4.870×10^{-3}
	ε_t	3.167×10^{-3}	4.472×10^{-3}	6.603×10^{-3}	1.191×10^{-2}
	$\dot{\varepsilon}$	2.62×10^{-5}/h	3.51×10^{-5}/h	7.02×10^{-5}/h	6.32×10^{-4}/h
Lateral strain	ε_0	-1.731×10^{-4}	-6.798×10^{-4}	-1.667×10^{-3}	-4.900×10^{-3}
	ε_c	-4.682×10^{-4}	-9.171×10^{-4}	-3.123×10^{-3}	-2.049×10^{-2}
	ε_t	-6.413×10^{-4}	-1.597×10^{-3}	-4.791×10^{-3}	-2.539×10^{-2}
	$\dot{\varepsilon}$	-1.81×10^{-5}/h	3.81×10^{-5}/h	-1.31×10^{-4}/h	-2.62×10^{-3}/h

Table 3: Creep parameters of sample after oil erosion under different stress levels.

Strain	ε	$0.4\sigma_{ucs}$	$0.5\sigma_{ucs}$	$0.6\sigma_{ucs}$	$0.7\sigma_{ucs}$	$0.8\sigma_{ucs}$
Axial strain	ε_0	3.382×10^{-3}	4.765×10^{-3}	5.620×10^{-3}	9.897×10^{-3}	1.068×10^{-2}
	ε_{c1}	4.076×10^{-4}	1.904×10^{-4}	1.064×10^{-3}	3.779×10^{-4}	3.581×10^{-4}
	$\dot{\varepsilon}_1$	2.47×10^{-5}/h	1.36×10^{-5}/h	3.60×10^{-3}/h	1.56×10^{-5}/h	2.67×10^{-4}/h
	Mutation	2.685×10^{-4}	2.586×10^{-4}	1.541×10^{-3}	—	—
	ε_{c2}	3.184×10^{-4}	7.597×10^{-4}	1.243×10^{-3}	—	—
	$\dot{\varepsilon}_2$	4.21×10^{-5}/h	7.38×10^{-5}/h	5.07×10^{-5}/h	—	—
	ε_t	4.376×10^{-3}	5.212×10^{-3}	9.469×10^{-3}	1.027×10^{-2}	1.104×10^{-2}
Lateral strain	ε_0	-2.539×10^{-5}	-8.254×10^{-5}	-8.889×10^{-5}	-4.176×10^{-2}	-5.389×10^{-2}
	ε_{c1}	-5.715×10^{-5}	-6.349×10^{-6}	-1.269×10^{-5}	-1.212×10^{-2}	-2.952×10^{-3}
	$\dot{\varepsilon}_1$	-3.46×10^{-6}/h	-4.56×10^{-7}/h	-4.89×10^{-5}/h	-5.02×10^{-4}/h	-2.12×10^{-3}/h
	Mutation	—	—	-3.072×10^{-2}	—	—
	ε_{c2}	—	—	-9.232×10^{-3}	—	—
	$\dot{\varepsilon}_2$	—	—	-3.77×10^{-3}/h	—	—
	ε_t	-8.254×10^{-5}	-8.889×10^{-5}	-4.0×10^{-2}	-5.389×10^{-2}	-5.684×10^{-2}

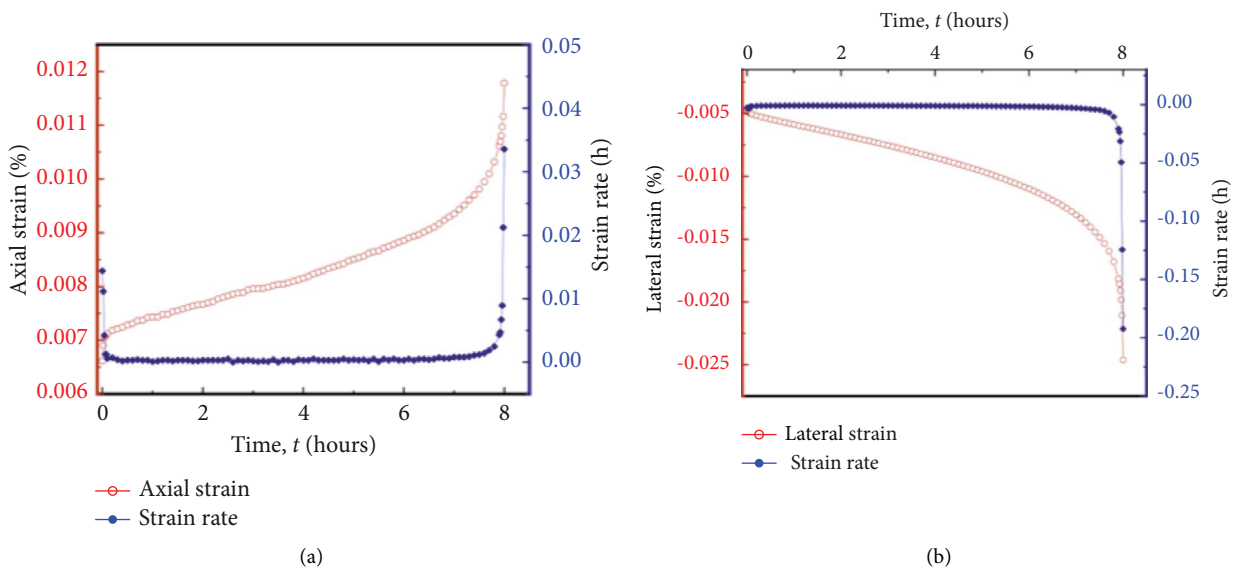

Figure 6: Creep strain and the associated creep strain rate of the natural sample at the final stress level.

natural sample is corroded by oil, the oil gradually penetrates into the pores of the sample and the contact surface between particles. It causes a reaction with the clay mineral particles inside the mudstone interlayer, so that the mudstone interlayer and the salt rock particles weaken the cementation, and the integrity of the structure is destroyed.

The axial creep strain of a sample after oil erosion is sourced from two parts: one part is the strain of internal mineral particles, while the other part is the strain of internal pore compaction. This is also the fundamental reason for the deterioration of the mechanical properties of the sample after oil erosion. In the accelerated creep stage, the lateral creep rate of the sample after oil erosion is greater than that of the natural sample, and the absolute value of the lateral creep rate of the two sets of samples is greater than the axial strain rate. In the stage approaching failure, the lateral creep rate change value is more sensitive than that of the axial strain rate change.

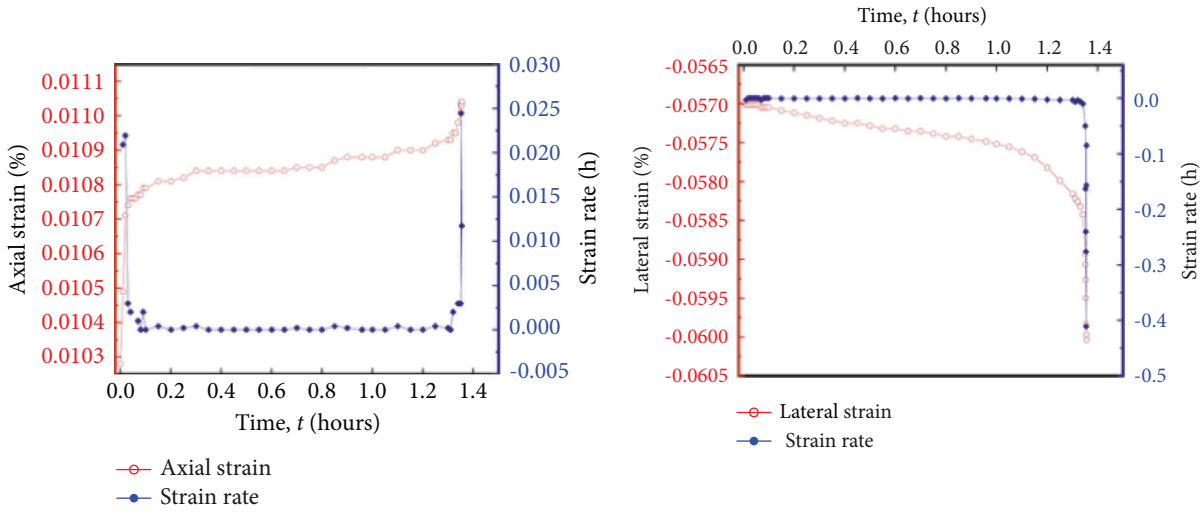

Figure 7: Creep strain and the associated creep strain rate of the sample after oil erosion at the final stress level.

3.1.3. Critical Stress Level for Creep Failure. Tables 2 to 3 show that the contribution of creep to samples deformation increased with the increase of stress level, and there is a critical stress level, demarking the beginning of a significant increase in creep strain. Studying the critical stress level of the mudstone interlayer is of great significance to the long-term operation condition design of the salt cavern oil storage. A variable to quantify the ratio of creep strain (ε_c) to total strain (ε_t) is defined, which is expressed as [24]

$$\beta = \frac{\varepsilon_c}{\varepsilon_t} \times 100. \quad (2)$$

From Equation (2), an increase in β represents an increase in creep performance, and a decrease in β represents a decrease in creep performance.

Figure 8 shows the β value of the natural sample and the sample after oil erosion at each stress level. For natural sample, whether it is axial creep strain or lateral creep strain, β decreased at low stress levels (loading ratios of 0.4 to 0.5). With the increase in the stress level, the β value kept increasing, and the higher the stress level, the larger the β value. The change law of the two shows consistency. For the sample after oil erosion, the β first increased and then decreased with the increase of the stress level for the axial creep strain. In Figure 8(b), there is a critical point (when the loading ratio is 0.6), and the curve is divided into two parts: an increasing part and a decreasing part. Before the critical point, the creep strain (ε_c) increased significantly, causing β value to increase with the increase of the stress level, which increased to 46.34% at one time. After this critical point (when the loading ratio is 0.6), the creep strain decreased significantly, causing β value to drop rapidly along with the stress level. In the sample after oil erosion, for the change of lateral creep, the change trend of β is roughly consistent with the axial creep. When the loading ratio reaches 0.5, the β value of axial creep increases, but the β value of lateral strain decreases significantly. This is because when the stress level is low (the loading ratio is 0.4~0.5), the main corrosion parts of the sample are gradually compacted or even crushed. In the whole creep process (the loading ratio is 0.4~0.7), the creep strain is mainly concentrated here, which is consistent with the results of the previous analysis. The critical point of the stress of the sample after oil erosion is $0.6\sigma_{ucs}$ (also a dangerous point). According to previous research on the creep test, when the stress level is lower than the threshold value (critical point), the damage is short-term and insignificant, but when the stress level exceeds the threshold value, damage will occur [24]. When the load ratio is 0.6, the β values of axial creep and lateral creep of the sample after oil erosion are 46.34% and 99.9%, respectively, and the β value of lateral creep is much larger than that of axial creep. Therefore, when the stress level is at a critical point for a long time, the proportion of lateral creep in the creep process is much higher than that of axial creep.

According to Figure 8, the critical stress level can be determined by a multistage creep test. The results show that long-term consideration of stress levels below 60% of peak strength is safe. The results show that it is safe to consider stress levels below 60% of peak strength in the long term. Beyond this point, the creep rate of the mudstone interlayer depends on the stress level and the operating conditions of the salt cavern oil storage.

3.1.4. Instantaneous Deformation Modulus. Since this test adopts the method of stepwise loading of stress levels, the pores of the samples are gradually compacted during the loading stage of each level of stress. Accordingly, the samples appear to have been hardened first and then damaged. In order to analyze the changes in the mechanical mechanism during the entire creep process, the instantaneous deformation modulus under the action of each stress level is studied.

The Hooke elastic model is used, and its constitutive equation is written as

$$\sigma = E\varepsilon. \quad (3)$$

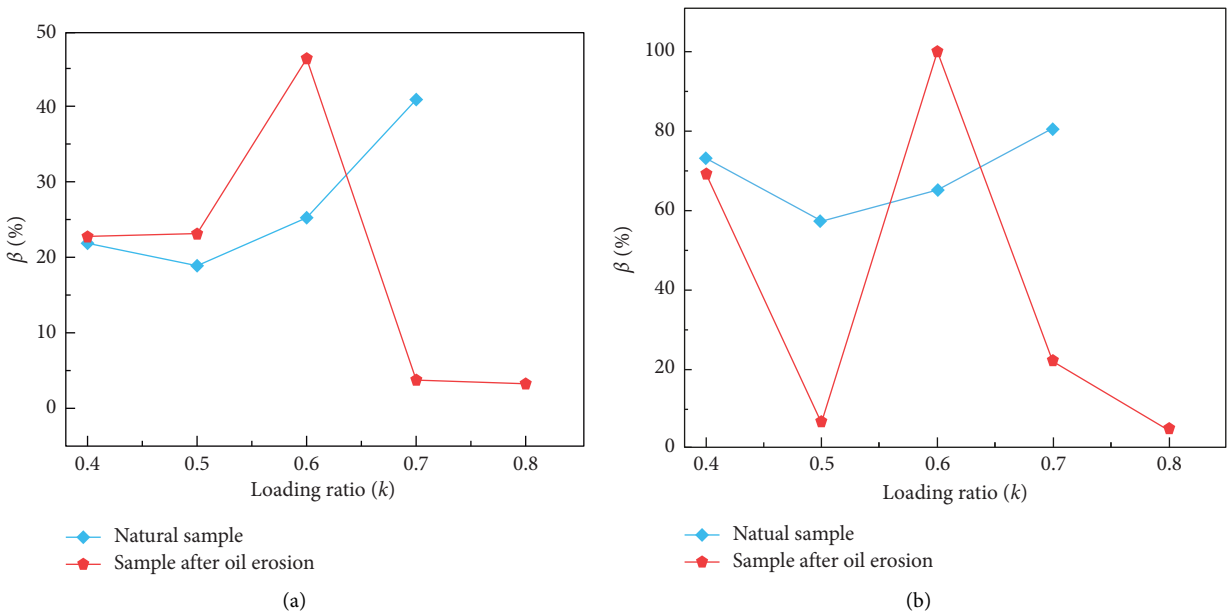

Figure 8: Relationship between β and the stress level (k).

From Equation (3), the instantaneous deformation modulus can be obtained as

$$E_m = \frac{\Delta\sigma}{\Delta\varepsilon} = \frac{\sigma_b - \sigma_a}{\varepsilon_b - \varepsilon_a}, \tag{4}$$

where E_m is the instantaneous deformation modulus, σ_a is the initial stress at each loading level, σ_b is the stress after each loading level is stable, ε_a is the axial strain when the stress is σ_a, and ε_b is the axial strain when the stress is σ_b.

Figure 9 shows the relationship between the deformation modulus and the loading ratio during the stress loading process. The change trend of the deformation modulus of the natural sample and the sample after oil erosion are the same. However, the deformation modulus of a natural sample is higher than that of a sample after oil erosion. When the loading ratio is between 0.4 and 0.5, the deformation modulus increases, and the increase of the sample after oil erosion is greater than that of the natural sample. The deformation modulus decreased as the loading ratio increased. However, when the stress level reaches the last level (that is, when the loading ratio of the natural sample is 0.7 and the loading ratio of the sample after oil erosion is 0.8), the deformation modulus has an increasing trend.

This change trend of the deformation modulus indicates that the mechanical mechanism of the sample has also changed correspondingly under different stress levels. Therefore, when the loading ratio is 0.4 to 0.5, the original pores inside the sample are gradually compacted and the internal microcracks are gradually closed. As the stress level increases, the internal pores are gradually compacted, which increases the load-bearing capacity of the sample and reduces the amount of deformation. When the loading ratio reaches the last level, its internal structure is severely damaged, and internal cracks continue to grow and develop, which increases the amount of deformation and then slightly increases the deformation modulus.

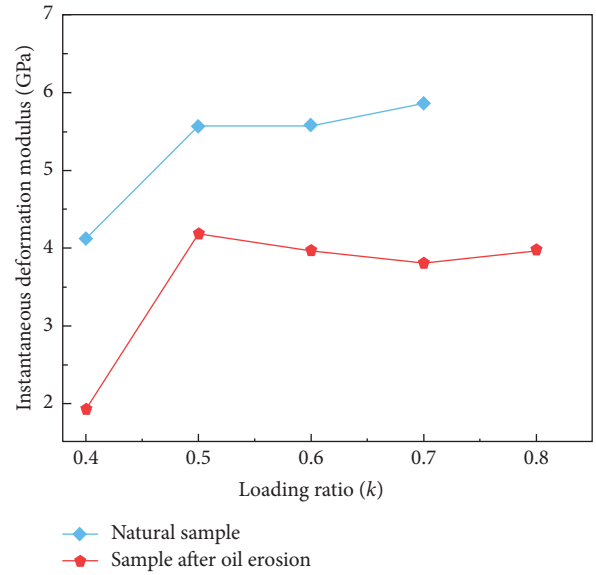

Figure 9: The relationship curve between the deformation modulus and the loading ratio during the creep process.

3.2. Acoustic Emission Characteristics. Under the action of an external load, the strain energy stored in the rock is released instantaneously to generate elastic waves, causing internal cracks to initiate, expand, and generate AE signals. AE signals can reflect the evolution of microcracks inside the rock [25]. Therefore, in the test process, the AE technology is used to monitor the damage characteristics of the rock during the creep process. However, due to the limitations of the experiment, the entire process of the creep experiment cannot be monitored in real time; only part of the AE signal can be monitored. Under each stress loading level, AE is used to monitor the damage characteristics of rock from initial loading to stable creep.

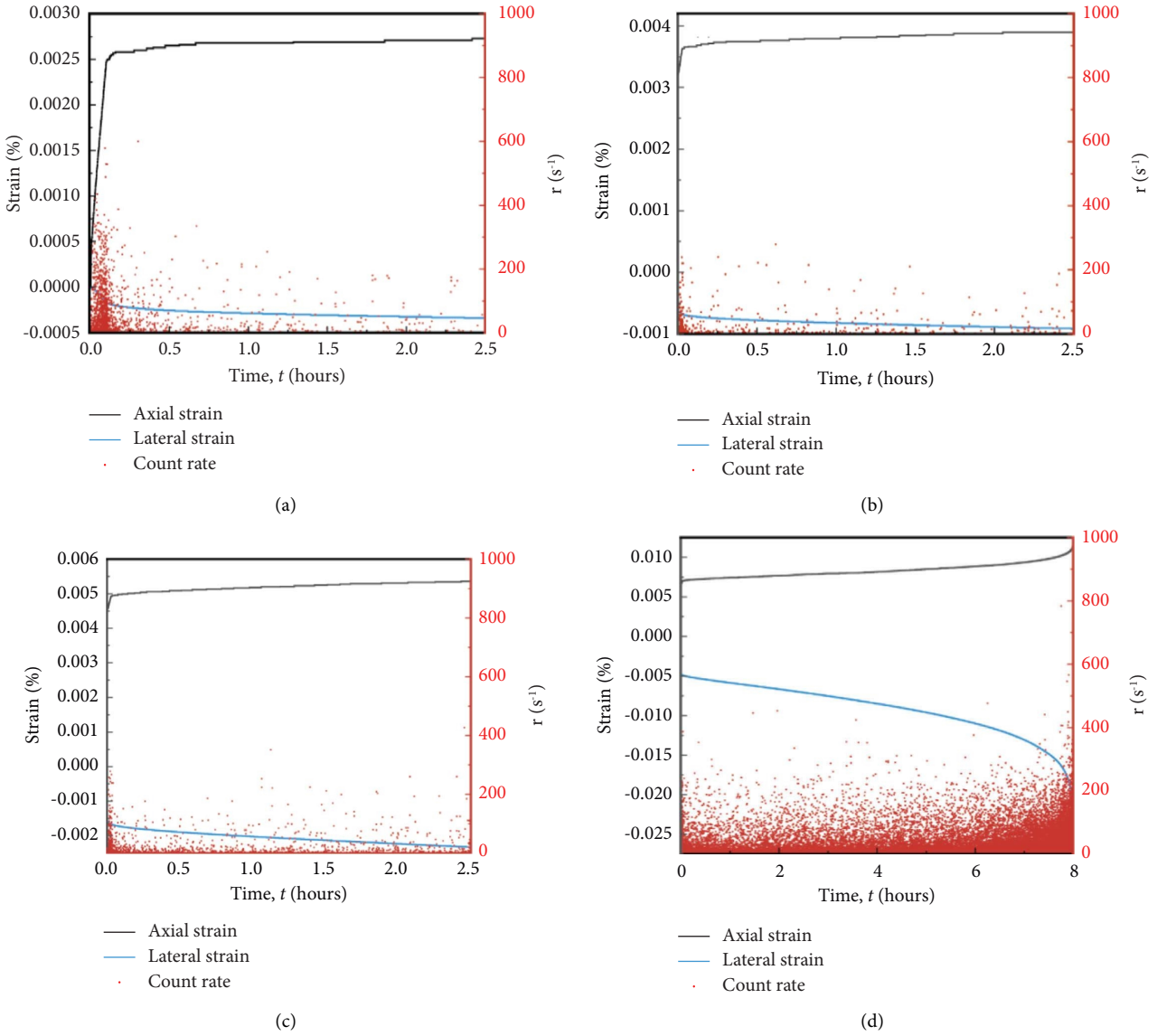

FIGURE 10: The relationship between the loading time, strain, and AE signal of the natural sample at each loading stage. (a) $0.4\sigma_{ucs}$. (b) $0.5\sigma_{ucs}$. (c) $0.6\sigma_{ucs}$. (d) $0.7\sigma_{ucs}$.

Figures 10 and 11 show the relationship between the loading time, strain, and AE signal of the natural sample and the sample after oil erosion, respectively. It can be seen that the natural sample and the sample after oil erosion have a certain degree of damage at each loading stage. A large number of AE signals were generated during the initial loading stage of each stress level. After the creep is stabilized, the AE signal is significantly reduced, and the last stage stress level generates a large number of AE signals throughout the stage. When the stress loading level is $0.4\sigma_{ucs}$, the AE signal generated by the natural sample is significantly higher than at other stress levels (except the last stress level). This shows that at the initial stage of loading, the initial microcracks or pores inside the sample are gradually squeezed and closed, producing damage and many AE signals. When the stress level is stabilized, the elastic strain caused by the imbalance between the crystal grains has enough time to coordinate with each other. Therefore, there will not be a large number of AE signals as in the initial stage of loading, and only a small amount of weaker AE signals will appear. However, as the stress level rises, the sample behaves approximately elastically, and the elastic deformation that is accumulated instantaneously will have a certain rebound recovery space due to the rapid generation of cracks and voids, and no new cracks will occur [26]. When the stress loading level is at the last level, the internal cracks of the sample develop rapidly, the internal structure is unstable and damaged, and a large number of AE signals are generated.

Comparing Figure 10 with Figure 11, it can be seen that the sample weakened significantly after being corroded by oil. In the loading stage of each stress level, the AE signals generated by the natural sample were significantly higher than those generated by the sample after oil erosion. When the stress is stabilized, the natural sample produced a small

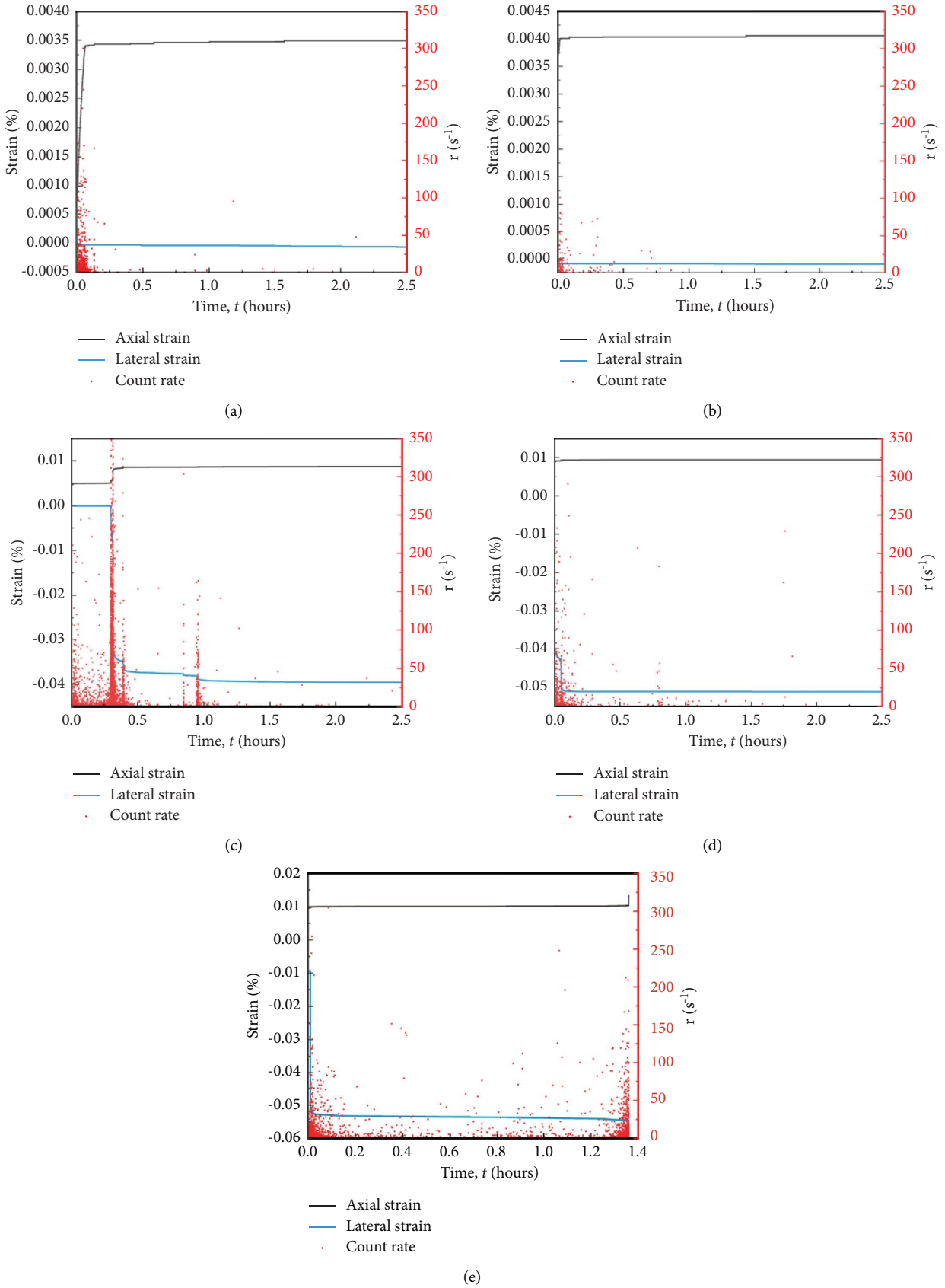

Figure 11: The relationship between the loading time, strain, and AE signals of the sample after oil erosion at each loading stage. (a) $0.4\sigma_{ucs}$. (b) $0.5\sigma_{ucs}$. (c) $0.6\sigma_{ucs}$. (d) $0.7\sigma_{ucs}$. (e) $0.8\sigma_{ucs}$.

amount of AE signals due to continuous adjustment of the elastic strain of the internal crystal grains. When the sample is eroded by oil, some of the internal mineral particles are eroded, resulting in many or even larger cracks and holes. Since the distance between the particles is large and the contact area is small, the elastic strain generated between the crystal grains has enough space to balance and adjust, so the friction between the mineral particles and the internal cracks is less. Many mineral particles react and migrate with the petroleum acid (naphthenic acid) in the oil, causing the cementation between them to become friable. This also explains microscopically why the AE signals of the sample will be significantly reduced after oil erosion. It is worth noting that in Figure 11(c), the sample after oil erosion produced a large number of AE signals at the moment of strain mutation. This also shows that at the moment of the strain mutation, it is also accompanied by the instantaneous collision between the large internal cracks and the squeezing and closing of the pores and the mineral particles because the captured AE signals are the elastic energy released by the internal microstructure failure [26–28]. Therefore, the large reduction of the AE signals reveals that a large amount of damage has been produced inside the sample after being corroded by the oil [29].

3.3. Analysis of Microscope Mechanism before and after Oil Erosion. The analysis above shows that after the sample is eroded by oil, the internal mineral particles are eroded, resulting in more cracks and pores. In order to better explain this phenomenon from a microscopic point of view, the microstructure of natural samples and samples after oil erosion was studied by scanning electron microscopy (SEM).

Figure 12 shows the microscopic observation results of natural samples and a sample after oil erosion. For the natural sample without oil erosion, when viewed at low magnifications, the mutual cementation between mineral particles is more compact, indicating that the sample has good integrity. With the increase in magnification, there are some cracks between the mineral particles, and a few salt particles adhere to the surface. When magnification was increased 6000 times, the cracks between the particles gradually appeared, but the size of these cracks is very small. In general, the particles are still closely embedded, and many salt particles are attached to the crack surface. To a certain extent, the capillary resistance is increased and the permeability of the sample is reduced.

For the natural sample eroded by oil, the sample gradually eroded from the outside to the inside. It can be seen that there is a clear boundary between the severely eroded area and the weakly eroded area on the sample surface: the particles in the severely eroded area are loose, while the particles in the weakly eroded area are dense.

In order to better understand the erosion mechanism, this article has made further microscopic observations on the typical microstructure of the erosion zone. It can be seen from the microscopic observation comparison images shown in Figure 12 that the microscopic observation of the severely eroded area has more microscopic cracks and pores than the weakly eroded area, and the cementation between the particles is looser. In the severely eroded area, the mineral particles are large and distributed in flakes, with obvious cracks and holes, and the microstructure is relatively loose. This also explains, from the microscopic perspective, that in the entire creep process, the severely corroded area of the specimen is also the main concentrated area of creep strain.

4. Analysis of the Deterioration Mechanism of Oil-Mudstone Interaction

4.1. Chemical Damage Mechanism. The creep test results show that the oil has an obvious influence on the deterioration of the mechanical properties of the interlayer. The change in macromechanical properties of the interlayer after oil erosion is due to the change in its internal microstructure (including the composition, size, shape, and contact mode of mineral particles). During the operation of the salt cavern oil storage, the acidic substance in oil (petroleum acid) reacts with the calcium sulfate in the interlayer of the oil phase to generate calcium naphthenate, which dissolves in the oil [30]. The reaction equation is

$$C_nH_{2n-1}COO^- + Ca^{2+} \longrightarrow (C_nH_{2n-1}COO)_2Ca. \quad (5)$$

The reaction between petroleum acid and calcium sulfate (mainly anhydrite) in the interlayer is the main reason for the damage and deterioration of the interlayer, which causes damage to the physical and mechanical properties of this part of the particle skeleton, resulting in the dissolution of pores. In addition, the reaction products exist in the form of ions, and some of the reaction products precipitate out of the interlayer along with the flow of the solution, thus increasing the porosity in the rock and changing the macroscopic mechanical properties of the interlayer.

4.2. Physical Damage Mechanism. The interlayer deterioration caused by the acidic substances in oil (petroleum acid) leads to a reduction of the bonding force between mineral particles and the friction between the particles or fractures. The pore pressure produced by the oil reduces the compressive stress between particles, which leads to the splitting of micropores and the damage and degradation of mechanical properties.

4.3. Dissolution-Migration Process of Interlayer Particles of Oil-Mudstone Interaction. The deterioration process of the interlayer of oil-mudstone interaction includes the dissolution of the interlayer particles and the migration of the liquid phase after the dissolution. On the basis of a literature study [31, 32], the dissolution process of interlayer particles under oil-rock action can be shown in Figure 13. The stress inside the interlayer is σ_{ij}, the stress acting on the interlayer surface is σ_n, the pressure produced by the oil is p, and the flow rate is u.

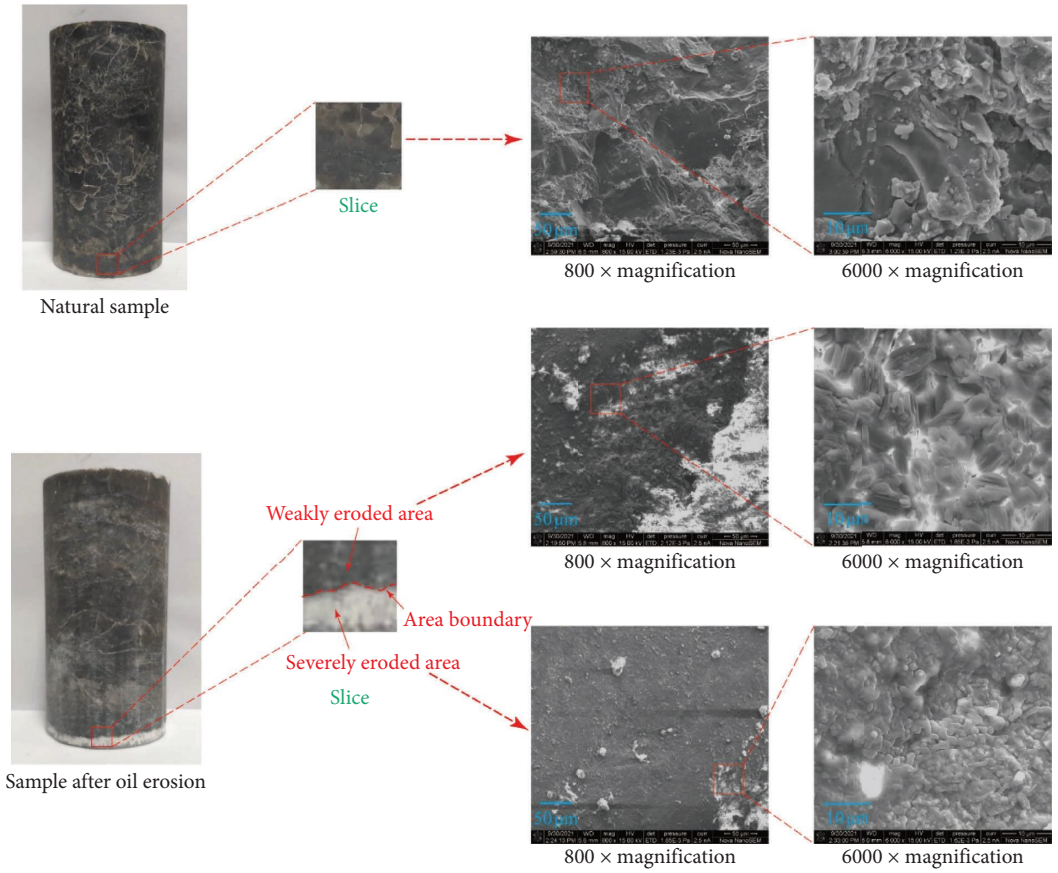

Figure 12: Analysis of microscope mechanism before and after oil erosion.

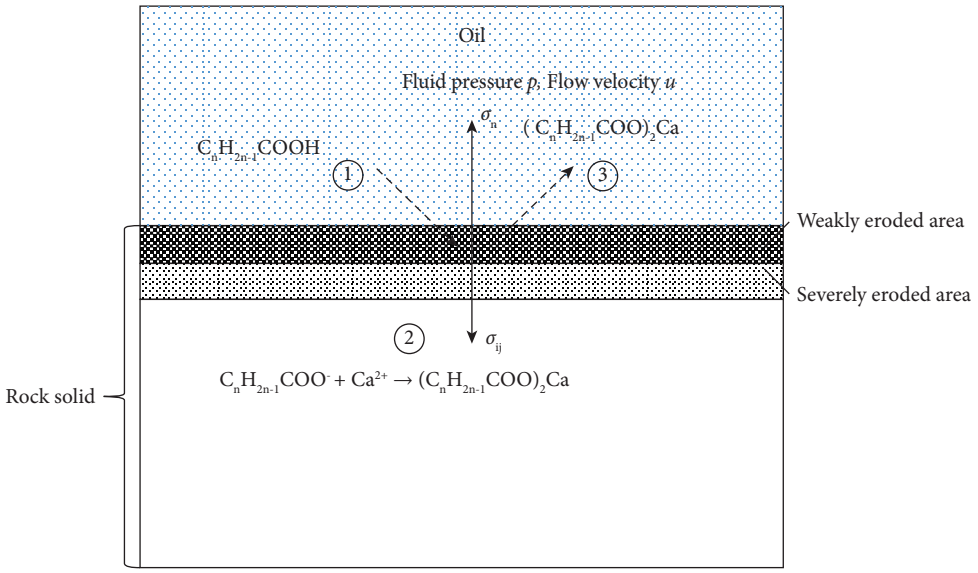

Figure 13: Deterioration process of interlayer under oil-mudstone interaction.

The process of dissolution and migration of interlayer particles under oil-mudstone interaction can be divided into three stages:

(1) The external oil transports petroleum acid molecules or H^+ to the interlayer surface through physical movements such as convection or diffusion (the first stage in Figure 13).

(2) The interlayer mineral grains undergo chemical reactions under the action of oil-rock (the second stage in Figure 13), resulting in the dissolution of pores (e.g., erosion zones).

(3) The reaction product (calcium naphthenate) is dissolved in oil by diffusion movement.

It is worth noting that in the second stage, the interlayer mineral particles react chemically under the action of oil-rock to form dissolved pores, which make the reaction further penetrate the rock sample. Due to the different degrees of internal and external erosion, the erosion area can be divided into a serious erosion area in contact with oil and a weak erosion area in the interlayer.

5. Conclusions

In order to explore the influence of oil on the mechanical properties of the interlayer around caverns during the operation of the salt cavern oil storage, the interlayer from the salt mines in Jiangsu was treated with oil erosion (under the condition of a pore pressure of 5 MPa). Multistage creep tests were carried out on the natural sample and the sample after oil erosion, respectively. The main conclusions are as follows:

(1) During the operation of the salt cavern oil storage, the naphthenic acid in the oil has a significant deterioration role on the compressive strength of the interlayer. After the interlayer is eroded by oil (under the condition of a pore pressure of 5 MPa), the failure duration is short, and the transition period from stable creep to accelerated creep is not obvious, showing obvious brittle failure characteristics.

(2) After the interlayer is eroded by oil, its lateral creep is not obvious at a low stress level (the loading ratio is 0.4~0.5), which is less than the axial creep deformation. At the last level of stress (the loading ratio is 0.8), the lateral creep is significantly higher than the axial creep.

(3) The critical stress level for creep failure of interlayers after oil erosion also changes, and the corresponding stress level is $0.6\sigma_{ucs}$. It is recommended that the long-term operating pressure of the salt cavern oil storage should be less than 60% of the peak strength of the interlayer after oil erosion.

(4) During the operation of the salt cavern oil storage, the oil migrates into the pores of the interlayer under the action of operating pressure, which further accelerates the reaction of petroleum acid and mineral particles, thereby accelerating the erosion of the surrounding rock. This is also the reason why the influence of operating pressure should be fully considered in the design of working conditions for salt cavern oil storage.

Taking the mudstone interlayer in the Jiangsu salt mining area as the research object, the change of the internal microstructure before and after oil erosion and the influence of oil erosion on the damage evolution and creep characteristics of the mudstone interlayer were studied. For engineering reference, bedded salt rocks in underground SPR caverns are in direct contact with petroleum during the operation. Petroleum erosion might weaken the physical and mechanical properties of interlayers. This could accelerate the damage to the surrounding rocks, affecting the stability and sealing ability of the reservoir as well as making its safety status unpredictable. However, during the operation of the underground SPR cavern in bedded rock salt, the oil leakage and migration laws and the deterioration process are still unclear, which is also a shortcoming of this paper. Therefore, in order to better provide a certain reference for the operation of the salt cavern oil storage, this part needs to be further studied in future work.

Abbreviations

k: Loading ratio
σ_a: Loading stress
σ_{ucs}: Uniaxial compressive strength
ε_0: Instantaneous strain
ε_c: Creep strain
ε_t: Total strain
ε_{c1}: Creep strain before mutation at the same stress level
ε_{c2}: Creep strain after mutation at the same stress level
$\dot{\varepsilon}$: Steady state creep strain rate
$\dot{\varepsilon}_1$: Creep strain rate before mutation at the same stress level
$\dot{\varepsilon}_2$: Creep strain rate after mutation at the same stress level
β: Critical stress level
σ: Stress
E: Young's modulus
ε: Strain
E_m: Instantaneous deformation modulus
σ_n: Stress acting on the interlayer surface
σ_{ij}: Stress inside the interlayer
p: Fluid pressure
u: Flow rate.

Data Availability

The data used to support the findings of this study are included within the article.

Disclosure

The paper has been read and approved by all authors.

Conflicts of Interest

The authors declare that they have no conflicts interest.

Authors' Contributions

He Chen and Huihua Peng contributed equally to this work.

Acknowledgments

The authors gratefully acknowledge the financial support provided by the Hunan Province Education Department (grant nos. 21B0664, 19B125, 20C0497, 19B124, and 21A0462) and the Hunan Institute of Engineering (grant nos. 21RC025 and XJ2005).The project was also funded by the Key R&D Project of Hunan Province Intelligent Disaster Prevention-Mitigation and Ecological Restoration in Civil Engineering (grant no. 2020SK2109).

References

[1] G. Wu, Y. M. Wei, C. Nielsen, X. Lu, and M. B. McElroy, "A dynamic programming model of China's strategic petroleum reserve: general strategy and the effect of emergencies," *Energy Economics*, vol. 34, no. 4, pp. 1234–1243, 2012.

[2] X. B. Zhang, Y. Fan, and Y. M. Wei, "A model based on stochastic dynamic programming for determining China's optimal strategic petroleum reserve policy," *Energy Policy*, vol. 37, no. 11, pp. 4397–4406, 2009.

[3] W. Liu, Z. Zhang, J. Chen, J. Fan, D. Jiang, and Y. Li, "Physical simulation of construction and control of two butted-well horizontal cavern energy storage using large molded rock salt specimens," *Energy*, vol. 185, pp. 682–694, 2019.

[4] W. Liu, Z. Zhang, J. Fan, D. Jiang, and Z. Li, "Research on gas leakage and collapse in the cavern roof of underground natural gas storage in thinly bedded salt rocks," *Journal of Energy Storage*, vol. 31, Article ID 101669, 2020.

[5] J. Chen, D. Lu, W. Liu, J. Fan, and D. Jiang, L. Yi, Y. Kang, Stability study and optimization design of small-spacing two-well (SSTW) salt caverns for natural gas storages," *Journal of Energy Storage*, vol. 27, Article ID 101131, 2020.

[6] B. Ehgartner and S. Sobolik, "Analysis of cavern shapes for the strategic petroleum reserve," *Tech Rep*, vol. 1, no. 1, pp. 3–44, 2006.

[7] N. Zhang, X. Shi, T. Wang, C. Yang, W. Liu, and H. Ma, "Stability and availability evaluation of underground strategic petroleum reserve (SPR) caverns in bedded rock salt of Jintan, China," *Energy*, vol. 134, pp. 504–514, 2017.

[8] T. Wang, C. Yang, X. Shi, H. Ma, Y. Li, and Y. Yang, "Failure analysis of thick interlayer from leaching of bedded salt caverns," *International Journal of Rock Mechanics and Mining Sciences*, vol. 73, pp. 175–183, 2015.

[9] X. Shi, Q. Chen, H. Ma, Y. Li, T. Wang, and C. Zhang, "Geomechanical investigation for abandoned salt caverns used for solid waste disposal," *Bulletin of Engineering Geology and the Environment*, vol. 80, no. 2, pp. 1205–1218, 2021.

[10] J. Fan, W. Liu, D. Jiang, J. Chen, and W. N. Tiedeu, "Time interval effect in triaxial discontinuous cyclic compression tests and simulations for the residual stress in rock salt," *Rock Mechanics and Rock Engineering*, vol. 53, no. 9, pp. 4061–4076, 2020.

[11] Y. Li, J. Liu, and C. Yang, "Influence ofmudstoneinterlayeron deformation and failure characteristics of salt rock," *J Rock MechEng25*, vol. 25, no. 12, pp. 2461–2466, 2006.

[12] F. Chen, Y. Li, C. Yang, and C. Zhang, "Experimentalstudy oncreep behaviors of rock salt in Yun Ying salt mine," *J Rock MechEng25*, vol. 25, no. S1, pp. 3022–3027, 2006.

[13] L. Wei, C. Jie, J. Deyi, S. Xilin, L. Yinping, and J. Daemen, "Tightness and suitability evaluation of abandoned salt caverns served as hydrocarbon energies storage under adverse geological conditions (AGC)," *Applied Energy*, vol. 178, pp. 703–720, 2016.

[14] J. Slizowski and L. Lankof, "Salt-mudstones and rock-salt suitabilities for radioactive-waste storage systems: rheological properties," *Applied Energy*, vol. 75, no. 1-2, pp. 137–144, 2003.

[15] Y. Li and C. Yang, "Three-dimensional expanded Cosserat medium constitutivemodel for laminated salt rock," *Rock Soil Mech*, vol. 27, no. 04, pp. 509–513, 2006.

[16] H. Zhou, C. Wang, B. Han, and Z. Duan, "A creep constitutive model for salt rock based on fractional derivatives," *International Journal of Rock Mechanics and Mining Sciences*, vol. 48, no. 1, pp. 116–121, 2011.

[17] C. Yang, T. Wang, Y. Li, H. Yang, J. Li, and D. Qu, Y. Yang and J. K. Daemen, Feasibility analysis of using abandoned salt caverns for large-scale underground energy storage in China," *Applied Energy*, vol. 137, pp. 467–481, 2015.

[18] X. Shi, Y. Li, C. Yang, and D. Qu, "Teststudyof influence of brineonten silestrength of muddy intercalation," *J Rock MechEng*, vol. 28, no. 11, pp. 2301–2308, 2009.

[19] N. Zhang, C. Yang, X. Shi, T. Wang, H. Yin, and J. Daemen, "Analysis of mechanical and permeability properties of mudstone interlayers around a strategic petroleum reserve cavern in bedded rock salt," *International Journal of Rock Mechanics and Mining Sciences*, vol. 112, pp. 1–10, 2018.

[20] X. Zhu and S. Tian, *Processes Development for Processing Highly Acidic Crude Oils*, Corrosion & Protection in Petrochemical Industry01, vol. 21, pp. 7–10, 2005.

[21] J. Chen, H. Chen, F. Wu et al., "Creep properties of mudstone interlayer in bedded salt RockEnergy storage based on multistage creep test: a case study of Huai'an salt mine," *Jiangsu Province, Geofluids*, vol. 2022, Article ID 2012776, 13 pages, 2022.

[22] H. Cheng, X. Zhou, X. Pan, and F. Berto, "Damage analysis of sandstone during the creep stage under the different levels of uniaxial stress using NMR measurements," *Fatigue and Fracture of Engineering Materials and Structures*, vol. 44, no. 3, pp. 719–732, 2021.

[23] C. Yang, J. Daemen, and J. H. Yin, "Experimental investigation of creep behavior of salt rock," *International Journal of Rock Mechanics and Mining Sciences*, vol. 36, no. 2, pp. 233–242, 1999.

[24] C. Yu, S. Tang, C. Tang et al., "The effect of water on the creep behavior of red sandstone," *Engineering Geology*, vol. 253, pp. 64–74, 2019.

[25] J. Chen, *Catastrophic Mechanism Induced by Damaged Surrounding Rock and Mitigation Principle during Bedded Salt Cavern Construction Period*, Chongqing University, Chongqing, China, 2012.

[26] Y. Kang, J. Chen, D. Jiang, W. Liu, and J. Fan, F. Wu, C. Jiang, Damage self-healing property of salt rock after brine immersionunder different temperatures," *Rock Soil Mech*, vol. 40, no. 02, pp. 601–609, 2019.

[27] P. Ranjith, M. Fourar, S. Pong, W. Chian, and A. Haque, "Characterisation of fractured rocks under uniaxial loading states," *International Journal of Rock Mechanics and Mining Sciences*, vol. 41, no. 3, p. 361, 2004.

[28] P. Ranjith, D. Jasinge, S. Choi, M. Mehic, and B. Shannon, "The effect of CO_2 saturation on mechanical properties of Australian black coal using acoustic emission," *Fuel*, vol. 89, no. 8, pp. 2110–2117, 2010.

[29] X. Jiang, K. Qian, X. Wang, S. Gao, K. Xie, and D. Jiang, "Effect of supercritical CO_2 on mechanical properties of sandstone using acousticemission and NMR," *Rock Soil Mech*, vol. 39, no. 04, pp. 1355–1361, 2018.

[30] T. Meng, Y. Hu, Q. Fu, G. Feng, and P. Jin, "Experimental study on fracture toughness of gypsum interlayer in bedded rocksalt under corrosive environment and its weakening mechanisms," *Rock Soil Mech*, vol. 38, no. 07, pp. 1933–1942, 2017.

[31] L. Shen, X. Feng, P. Pan, and H. Zhou, "Chemical kinetics dissolution mechanism of rock under stress," *Rock Soil Mech*, vol. 32, no. 05, pp. 1320–1326, 2011.

[32] M. S. Paterson, "Nonhydrostatic thermodynamics and its geologic applications," *Reviews of Geophysics*, vol. 11, no. 2, pp. 355–389, 1973.